Time-evolution simulation of a controlled-NOT gate with two coupled asymmetric quantum dots

S. Moskal, S. Bednarek, and J. Adamowski*
Faculty of Physics and Applied Computer Science, AGH University of Science and Technology, Kraków, Poland
(Received 26 February 2005; published 21 June 2005)

We study a possible physical realization of a quantum controlled-NOT gate with the use of two weakly coupled asymmetric quantum dots. Solving the time-dependent Schrödinger equation for the model two-electron system, we simulate the infrared-radiation-induced quantum transitions that correspond to basic gate operations. We require the transition probabilities to be close to 1 and optimize the parameters of the nanostructure in order to make the gate operation time as short as possible. In the simulations, we have taken into account the entire energy spectrum, which can be populated by the absorption or emission of the infrared radiation. We discuss the consequences of the existence of many bound two-electron states on the probability of radiative transitions.

DOI: 10.1103/PhysRevA.71.062327 PACS number(s): 03.67.Lx, 03.67.Mn, 73.21.La

I. INTRODUCTION

In recent papers, one can find many theoretical proposals for the implementation of quantum dots (QDs) [1] in quantum computation [2–15]. These proposals consist in application of either the orbital or spin states of electrons confined in the QDs. The orbital states of electrons in the coupled QDs were proposed for a possible realization of a quantum controlled-NOT (CNOT) gate [2,5,7,9]. Spin states of coupled QDs are intensively studied [3,4,6,12] as possible candidates for qubits and quantum logic gates due to the long relaxation time of Zeeman-split states in an external magnetic field [16]. Performing a direct measurement, Hanson *et al.* [16] demonstrated that the relaxation time of the spin states of the QD-confined electrons is sufficiently long to use these states as qubits in quantum computation. Hayashi *et al.* [18] reported the coherent manipulation of spin qubits in laterally coupled QDs. The large number of theoretical papers on quantum computation with QDs, e.g., [2–4,6–13,15], is in contrast with the small number of experimental studies, e.g., [16–18]. The discrepancy between the numbers of theoretical and experimental papers mainly results from the decoherence problem [19]. In order to use the qubits as efficient information carriers and to perform a unitary time evolution of them we have to maintain the coherent quantum states for a time that exceeds by many orders of magnitude the quantum gate operation time. This requirement is very difficult to satisfy in solid-state devices.

The present work is an attempt to fill the gap between the existing theoretical treatments and experiment. For a system of coupled QDs we perform a direct numerical simulation of the quantum gate operation. We apply a theoretical model that possibly well reproduces the properties of the real nanostructure. In this model we can keep the coherent qubit states for an arbitrary long time and perform the unitary evolution of the qubits. We focus on the two-qubit CNOT gate, which together with all the one-qubit gates, constitutes a universal set of quantum logic gates [20]. For the purpose of implementation of the gate we have to find a physical realizations of the states of a computational basis and a unitary operator, which performs the CNOT logic gate. In the present model, the computational basis is composed from the four selected eigenstates of two electrons confined in two asymmetric QDs. The CNOT operation is realized with the help of an infrared radiation pulse with a proper duration time.

The implementation of the CNOT gate on the basis of coupled QDs was first proposed by Barenco *et al.* [2], who considered two symmetric QDs, in which the asymmetry was generated by an external electric field. The application of coupled asymmetric QDs to realize a CNOT gate was studied by Balandin and Wang [5], Sanders *et al.* [9], and Tanamoto [7]. In the papers [5,7,9] a one-dimensional model nanostructure is employed and the interaction between the electrons in different QDs is taken on in a simplified form as the dipole-dipole interaction [5,9]. Moreover, the authors [5,7,9] take into account only the lowest-energy states. In the present paper, we extend the model [2,5,9] to a three-dimensional nanostructure and take into account all the two-electron states with discrete energy levels in the energy interval of interest. We calculate the gate operation time, which is of crucial importance for the possible physical realization of QD-based quantum computation, and compare this time with the coherence time [19].

The paper is organized as follows: We present the theoretical model in Sec. II and the results of simulations in Sec. III, Sec. IV contains a discussion, and Sec. V conclusions and a summary.

II. THEORETICAL MODEL

We consider two electrons confined in two coupled asymmetric QDs. The barrier separating the QDs is taken to be sufficiently wide so that the tunneling of electrons between the individual QDs is neglected. Such a nanostructure can be formed, e.g., in a quantum wire, which is fabricated from different materials [21]. We assume that the nanostructure possesses cylindrical symmetry and lateral confinement of the electrons, i.e., the confinement in the x-y plane, perpendicular to the growth (z) axis, is much stronger than the

*Electronic address: adamowski@ftj.agh.edu.pl

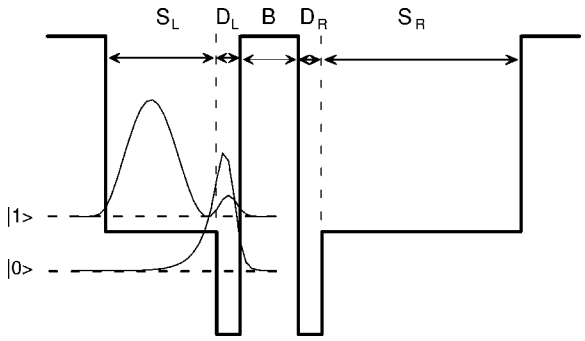

FIG. 1. Confinement potential profile in the vertical direction for two coupled QDs. Shown is also the electron probability density for the one-electron ground ($|0\rangle$) and first excited ($|1\rangle$) states. B is the barrier thickness, D_L (D_R) is the thickness of the deep potential-well region in the left (right) QD, and S_L (S_R) is the thickness of the shallow potential-well region in the left (right) QD.

vertical (z) confinement. The lateral confinement is approximated by a harmonic-oscillator potential and the vertical confinement has the form of asymmetric potential wells separated by the barrier (Fig. 1). Under these assumptions the three-dimensional eigenvalue problem can be reduced to a one-dimensional problem [22,23] with the effective electron-electron interaction

$$U_{eff}(z_1,z_2) = \frac{e^2\sqrt{\pi\beta}}{4\pi\epsilon_0\epsilon} e^{\beta|z_1-z_2|^2}\,\mathrm{erfc}(\sqrt{\beta}|z_1-z_2|), \qquad (1)$$

where z_1 and z_2 are the vertical coordinates of the electrons, ϵ is the relative electric permittivity of the QD material, $\beta = m_e\hbar\omega_\perp/2$, m_e is the effective electron band mass, and $\hbar\omega_\perp$ is the oscillator excitation energy for the lateral confinement [22,23]. The effective Hamiltonian of the two electrons confined in the two asymmetric QDs has the form [23]

$$H_0 = -\frac{\hbar^2}{2m_e}\left(\frac{\partial^2}{\partial z_1^2}+\frac{\partial^2}{\partial z_2^2}\right) + U_{conf}(z_1) + U_{conf}(z_2) + U_{eff}(z_1,z_2), \qquad (2)$$

where the ground-state energy of two noninteracting electrons in the lateral parabolic potential is taken on as the reference energy and $U_{conf}(z_i)$ is the vertical confinement potential energy of the ith electron. In each QD, the confinement potential is different (cf. Fig. 1), which allows us to distinguish the electrons localized in the left and right QDs. The single electron confined in the left QD will act as a control qubit and the electron confined in the right QD as a target qubit. Each QD consists of two regions with shallow and deep potential wells that have thicknesses S_L (S_R) and D_L (D_R), respectively. The values of the QD parameters taken in the present calculations are quoted in Table I. Figure 1 also shows the electron density for the single-electron states, the ground state $|0\rangle$ and first excited state $|1\rangle$, localized in the left QD.

TABLE I. Optimized values of the parameters of the model QD nanostructure.

Region	Thickness (nm)	Potential-well depth (meV)
S_L	19	200
D_L	4	305
B	10	0
D_R	4	305
S_R	27	200

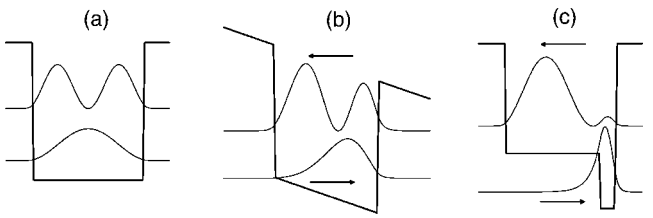

FIG. 2. Electron probability density for the one-electron ground and first excited states localized in (a) symmetric QD, (b) symmetric QD in an electric field, and (c) asymmetric QD. Arrows indicate the shift of the electron density in cases (b) and (c) with respect to case (a).

The asymmetry of the confinement potential leads to a shift of the electron density distribution with respect to the symmetric QD [cf. Figs. 2(a) and 2(c)]. In the even- and odd-parity states, the electron density is shifted in opposite directions, which causes different electron-electron interaction energy depending on the one-particle states occupied. We note that a similar effect can be obtained when applying an external electric field to the nanostructure [Fig. 2(b)]. However, the application of the electric field is disadvantageous since already the weak electric field can cause a leakage current, which empties the QD.

It appears that the two-electron system considered possesses many bound states with energy levels in the relevant energy regime (cf. Table II). The ground state of the system, denoted as $|00\rangle$, is the spin singlet. The gate operations will be realized by dipole radiative transitions, which do not change the spin of the electron. Therefore, we will consider only spin singlet states as candidates for the states of the

TABLE II. Energy levels E_ν of the ten lowest-energy states of the model two-electron system. ν numbers the subsequent energy levels. The lateral excitation energy $2\hbar\omega_\perp$ is included in E_ν. The computational-basis states $|ij\rangle$ are listed in the last column.

ν	E_ν (meV)	$\|ij\rangle$
1	−356.59	$\|00\rangle$
2	−342.15	
3	−342.02	
4	−329.81	$\|01\rangle$
5	−324.80	
6	−321.57	$\|10\rangle$
7	−313.98	
8	−307.86	
9	−301.09	
10	−293.34	$\|11\rangle$

TABLE III. Energy separations between energy levels E_{ij} of the computational-basis states $|ij\rangle$ and energy difference ΔE between the two transition energies relevant to the CNOT gate operation.

Energy difference	(meV)
$\Delta E_I = E_{01} - E_{00}$	26.78
$\Delta E_{II} = E_{11} - E_{10}$	28.23
$E_{10} - E_{01}$	8.24
$E_{10} - E_{00}$	36.47
$E_{11} - E_{01}$	35.02
$\Delta E = \Delta E_{II} - \Delta E_I$	1.45

computational basis. In simulations of the two-qubit CNOT gate, the computational-basis states, denoted by $|00\rangle$, $|01\rangle$, $|10\rangle$, and $|11\rangle$, have been chosen as the two-qubit states, which correspond to the occupation of each QD by a single electron. The state $|00\rangle$ corresponds to the occupation of one-electron ground states in different QDs, in state $|01\rangle$ ($|10\rangle$), the electron in the left QD is in the ground state (first excited state) and the electron in the right QD is in the first excited state (ground state), and in state $|11\rangle$ the electrons in both the QDs are in the first excited state. Table II shows that—in the energy range between the energy levels corresponding to the states $|00\rangle$ and $|11\rangle$—there are several discrete energy levels. For $\nu = 2$, 3, 5, 7, and 9 the energy levels are associated with bound states in which both the electrons are localized in the same QD. In the simple model [2] of the QD, these additional bound states were neglected. In the present paper, we will take into account the effect of these states on the possible quantum transitions.

In an asymmetric QD system, the Coulomb interaction energy between the electrons in the various states is different. This interaction energy depends on the occupation of the quantum states in the QDs. Therefore, the subsequent energy levels associated with the different two-electron states will be shifted upward on the energy scale by different values. This energy-level differentiation will play a crucial role in quantum-gate operation. The separations between the energy levels of the computational basis states are listed in Table III, in which E_{ij} $(i,j=0,1)$ denotes the energy of the computational-basis state $|ij\rangle$. We are interested in the following energy differences: $\Delta E_I = E_{01} - E_{00}$, $\Delta E_{II} = E_{11} - E_{10}$, and $\Delta E = \Delta E_{II} - \Delta E_I$. For reliable quantum-gate operation the energy difference ΔE should be sufficiently large in order to ensure the selective absorption of the electromagnetic radiation. According to the uncertainty principle, the shorter the time of transition between the considered states, the larger the misfit of the transition energies. In consequence, if there exist additional bound states with energy levels localized in the near neighborhood of the final-state energy level these additional states can be occupied with nonzero probability.

In the dipole approximation, the Hamiltonian of the interaction of the electrons with the electromagnetic wave is given by

$$H_{int} = A\cos(\omega t)\hat{p} = -i\hbar A\cos(\omega t)\left(\frac{\partial}{\partial z_1} + \frac{\partial}{\partial z_2}\right), \qquad (3)$$

where A is the electromagnetic wave amplitude, ω is the wave frequency, t denotes the time, and $\hat{p}$ is the operator of the z component of the total two-electron momentum. The time evolution of the two-electron system is determined by the total Hamiltonian $H = H_0 + H_{int}$.

The time of transition between two quantum states becomes shorter if the wave amplitude A increases. However, the amplitude A cannot be too large, since for large A we deal with a large spread of the energy of the electromagnetic wave, which leads to undesirable transitions to the neighboring states. Therefore, there exists an upper bound on the wave amplitude A, which results from the actual energy-level structure (cf. Table II). The existence of this upper limit on the wave amplitude A is disadvantageous, since it disables shortening of the gate-operation time, which is necessary to complete the possibly large number of gate operations within the coherence time [24]. In conclusion, it is of crucial importance for efficient gate operation that the energy levels are significantly differentiated. In particular, the energy levels associated with the computational-basis states should be distinctly separated.

Taking the above limitations into account we have optimized the shape of the confinement potential $U_{conf}(z)$ in order to obtain the energy-level structure that minimizes the time duration of the single quantum-gate working cycle. Additionally, we require the probability of quantum transitions between the initial and final states to be larger than 99.9%. We also note that the thickness of the barrier layer has to be limited from below in order to suppress the electron tunneling between the QDs. The values of parameters listed in Table I have been obtained from this optimization.

The two-electron bound states of Hamiltonian (2) have been calculated by the imaginary-time step method [25]. Accordingly, we start from the time-dependent Schrödinger equation

$$i\hbar\frac{\partial\psi(z_1,z_2,t)}{\partial t} = H_0\psi(z_1,z_2,t), \qquad (4)$$

introduce the imaginary variable $\tau = it$ into Eq. (4), and substitute the derivatives by the appropriate finite-difference approximations. A simple transformation leads to the following iterative procedure:

$$\psi^{n+1} = \psi^n - \frac{\Delta\tau}{\hbar}H_0\psi^n, \qquad (5)$$

where the index n labels the subsequent iterations, i.e., the subsequent imaginary-time steps. The time interval $\Delta\tau$ is chosen so that the iterative procedure is possibly fast and convergent. The iterative procedure (5) converges toward the ground-state wave function. The excited-state wave functions are found by the same procedure associated with the simultaneous orthogonalization of the currently calculated wave function to the previously found wave functions associated with the lower-energy levels.

The real-time evolution of the system is obtained if we substitute Eq. (5) by the iterative procedure [26], which is symmetric against time inversion, i.e.,

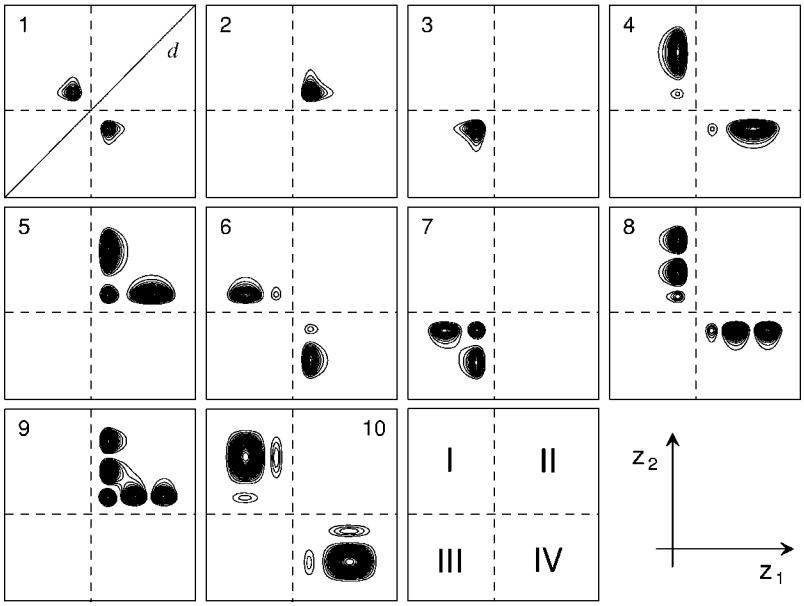

FIG. 3. Contours of the probability density for the ten lowest-energy states of the two-electron system in the coupled QD nanostructure. Dashed lines separate different quadrants; *d* denotes the diagonal.

$$\psi^{n+1} = \psi^{n-1} - 2i\frac{\Delta t}{\hbar}H\psi^{n}, \tag{6}$$

where H is the total Hamiltonian, which takes into account the interaction with the electromagnetic wave as given by Eq. (3).

We study the quantum CNOT gate, defined by the unitary operator U_{CNOT}, which acts on the computational-basis states as follows:

$$U_{\mathrm{CNOT}}|00\rangle = |00\rangle, \tag{7a}$$

$$U_{\mathrm{CNOT}}|01\rangle = |01\rangle, \tag{7b}$$

$$U_{\mathrm{CNOT}}|10\rangle = |11\rangle, \tag{7c}$$

$$U_{\mathrm{CNOT}}|11\rangle = |10\rangle. \tag{7d}$$

The operator U_{CNOT} changes the target qubit if and only if the control qubit is set to $|1\rangle$. The quantum CNOT gate possesses the important property of the creation of entangled quantum states, i.e.,

$$U_{\mathrm{CNOT}}(\alpha|0\rangle + \beta|1\rangle)|0\rangle = \alpha|00\rangle + \beta|11\rangle, \tag{8}$$

where $|\alpha|^2+|\beta|^2=1$. In the present paper, we will simulate the four operations defined by Eqs. (7a)–(7d) and the creation of the entangled state defined by Eq. (8).

III. RESULTS

The eigenfunctions ψ of Hamiltonian (2) depend on two spatial coordinates, which determine the positions of the two electrons, i.e., $\psi=\psi(z_1,z_2)$. Figure 3 shows the probability density, i.e., $\rho(z_1,z_2)=|\psi(z_1,z_2)|^2$, as a function of electron coordinates for the ten lowest-energy states. The probability density $\rho(z_1,z_2)$ is symmetric against the interchange of the electron positions, i.e., $\rho(z_1,z_2)=\rho(z_2,z_1)$. In Fig. 3 this symmetry is shown as reflection symmetry with respect to the diagonal *d*. In the computational-basis states, each electron should be localized in a different QD, which corresponds to the electron probability density localized in quadrants I and IV. This condition is satisfied by the states with numbers 1, 4, 6, 8, and 10. We choose states 1, 4, 6, and 10 (cf. Fig. 3 and Table II) as the computational-basis states, since they are constructed from the ground and first excited states of a single qubit (the state 8 corresponds to the second excited state). The states for which the electron probability density is localized in quadrants II and III correspond to the localization of both the electrons in the same QD (quadrant II in the right QD and quadrant III in the left QD).

According to Eq. (8), the CNOT gate produces the entangled state from the superposition of states. Figure 4 shows the two-electron wave function and electron probability density of the maximally entangled state, i.e.,

$$\frac{1}{\sqrt{2}}(|00\rangle + |11\rangle). \tag{9}$$

The profiles of the wave function along $z_2=a$ and b demonstrate that the entanglement condition is satisfied. This condition can be formulated as the following nonseparability condition:

$$\psi(z_1,z_2) \neq \phi(z_1)\phi(z_2), \tag{10}$$

where $\phi(z)$ is the one-electron wave function. If the state were unentangled, the following equality would be satisfied:

$$\psi(z_1,a) = \mathrm{const} \times \psi(z_1,b), \tag{11}$$

which is equivalent to the separability of the two-electron wave function into a product of one-electron wave functions.

In the following, we present the results of the simulations of the CNOT gate working cycles, defined by Eqs. (7a)–(7d), and the entanglement production, defined by Eq. (8). The CNOT gate operator can be formally written down as follows:

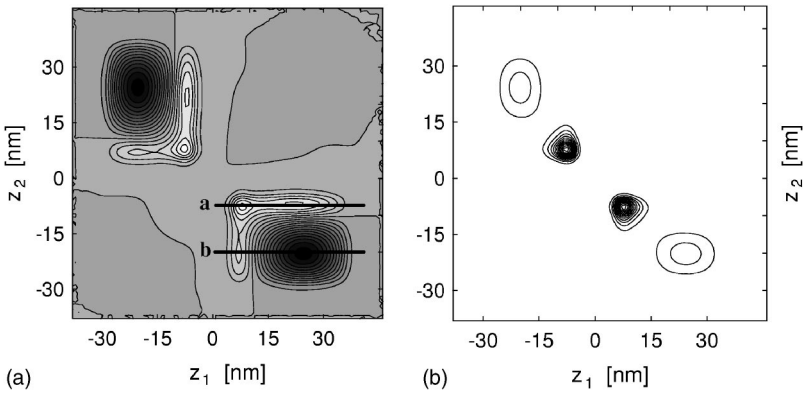

FIG. 4. Contour plots of the wave function (a) and the electron probability density (b) for the entangled state [Eq. (9)]. In (a) the values of the wave function are given in gray scale: the bright (dark) areas correspond to the positive (negative) wave-function values. A more detailed description is given in text.

$$U_{\mathrm{CNOT}} = \exp\left(-\frac{i}{\hbar}Ht\right), \tag{12}$$

where H is the total Hamiltonian of the two-electron system interacting with the electromagnetic wave with appropriately chosen frequency ω. In the simulations of the CNOT gate operation, we have chosen the π pulse with duration time t_π defined by

$$\frac{t_\pi A}{\hbar}|\langle 10|\hat{p}|11\rangle| = \pi, \tag{13}$$

and with a fixed frequency that corresponds to the energy difference ΔE_{II} between the energy levels associated with two-qubit states $|11\rangle$ and $|10\rangle$.

In order to enable a presentation of the time evolution of the two-qubit states, we integrate the two-particle probability density over one spatial coordinate and obtain the one-particle probability density

$$\rho_1(z_1,t) = \int_{-\infty}^{+\infty} dz_2 \rho(z_1,z_2,t), \tag{14}$$

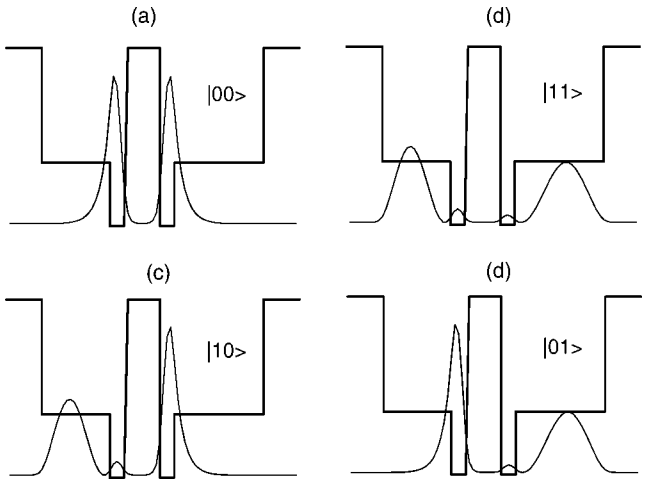

FIG. 5. One-electron probability density [Eq. (14)] for the computational-basis states for $t=0$. Also shown is the profile of the confinement potential.

where we have explicitly introduced the time dependence into the electron probability density. Figure 5 displays the one-electron probability density, i.e., $\rho_1(z_1,0)$, for the stationary states of the computational basis.

Figures 6–9 demonstrate the simulations of different outcomes of the CNOT gate [Eqs. (7a)–(7d)]. In Figs. 6–10, the abscissa corresponds to electron position z_1 and the ordinate corresponds to the time. The contour plots show the one-electron probability density $\rho_1(z_1,t)$.

In the present work, the simulation of the realization of each transformation, given by Eqs. (7a)–(7d) and (8), has been divided into three steps. During the first two steps (a) and (b) the required initial quantum state of the system is prepared, while step (c) corresponds to the CNOT gate operation. In step (a) the system relaxes to the ground state, denoted by $|00\rangle$. This relaxation process is simulated by the imaginary-time step method [note the different time scale used in parts (a) and (b), (c) in Figs. 6–10]. We need several hundreds of iterations in order to prepare the ground state, in which the electron probability density is mainly localized in the deep potential-well regions [cf. Figs. 5(a), 6(a), 7(a), 8(a), 9(a), and 10(a)]. Step (b) consists in the preparation of the initial state of the system [cf. Figs. 6(b), 7(b), 8(b), 9(b),

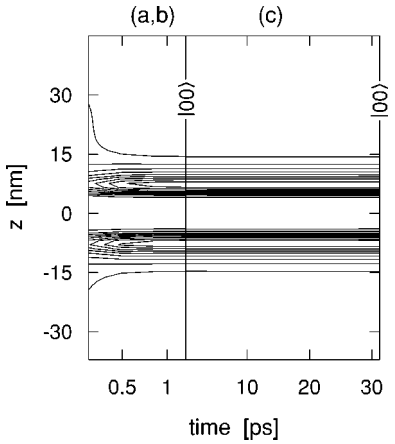

FIG. 6. Contour plots of the electron probability density as functions of time t and spatial coordinate $z=z_1$ for the working cycle of the CNOT gate corresponding to the operation defined by Eq. (7a). (a,b) corresponds to the relaxation of the system to the ground state and simultaneously the preparation of the initial state. (c) corresponds to the CNOT gate operation defined by Eq. (7a).

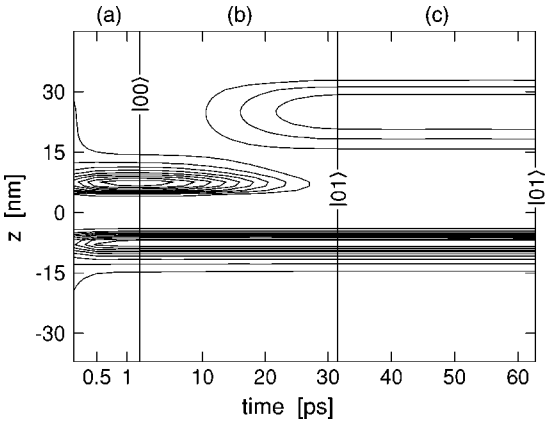

FIG. 7. Contour plots of the electron probability density as functions of time t and spatial coordinate $z=z_1$ for the working cycle of the CNOT gate corresponding to the operation defined by Eq. (7b). (a) relaxation to the ground state, (b) preparation of initial state $|01\rangle$, and (c) CNOT gate operation defined by Eq. (7b).

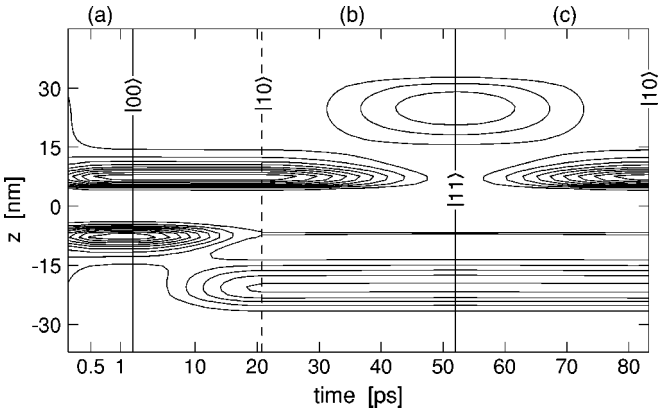

FIG. 9. Contour plots of the electron probability density as functions of time t and spatial coordinate $z=z_1$ for the working cycle of the CNOT gate corresponding to the operation defined by Eq. (7c). (a) Relaxation to the ground state, (b) two-step preparation of initial state $|11\rangle$, and (c) CNOT gate operation defined by Eq. (7d).

and 10(b)]. For the transformation given by Eq. (7a) the initial state is already prepared during the relaxation process [cf. Fig. 6(a) and 6(b)]. However, for the next three transformations given by Eqs. (7b)–(7d) the initial state is prepared with the help of the π pulse with frequency adjusted to the corresponding transition. Parts (b) of Figs. 7–9 show that electron density is transferred from the deep into the shallow potential-well region, which corresponds to the transition of one electron from the ground state to the first excited state. During this process the electron density of the second electron remains unchanged, i.e., this electron is still in the ground state. Figure 9(b) shows that the initial state $|11\rangle$ is prepared in two steps as a result of the transitions $|00\rangle \rightarrow |10\rangle \rightarrow |11\rangle$.

Having the system prepared in the initial state, we apply the π pulse with frequency $\omega=42.9$ THz, i.e., with photon energy $\hbar\omega$ exactly equal to the energy difference ΔE_{II} of the transition between the states $|10\rangle$ and $|11\rangle$. This π pulse realizes the CNOT gate operation [cf. Figs. 6(c), 7(c), 8(c), 9(c), and 10(c)]. The electromagnetic radiation with photon energy $\hbar\omega=\Delta E_{II}$ does not cause any transitions between states $|00\rangle$ and $|01\rangle$.

The production of the entangled state as a result of the CNOT gate is demonstrated in Fig. 10. In step (b) the system has been prepared in initial state $(|00\rangle+|10\rangle)/\sqrt{2}$ as a result of the absorption of the $\pi/2$ pulse with frequency adjusted to the transition $|00\rangle \rightarrow |10\rangle$. In step (c), we apply to the prepared initial state a π pulse that realizes the CNOT gate operation and produces the entangled state (cf. Fig. 4).

IV. DISCUSSION

Let us discuss the limitations on quantum gate operation with coupled QDs that result from the decoherence [19]. In

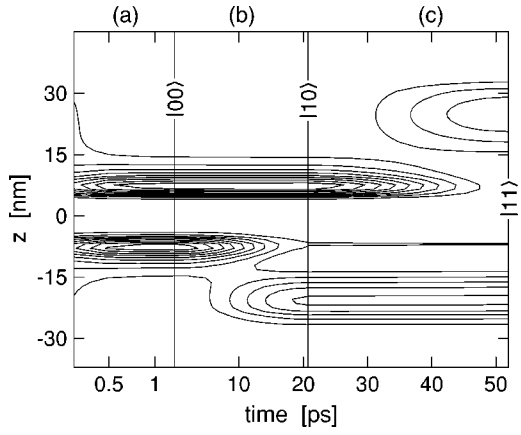

FIG. 8. Contour plots of the electron probability density as functions of time t and spatial coordinate $z=z_1$ for the working cycle of the CNOT gate corresponding to the operation defined by Eq. (7c). (a) Relaxation to the ground state, (b) preparation of initial state $|10\rangle$, and (c) CNOT gate operation defined by Eq. (7c).

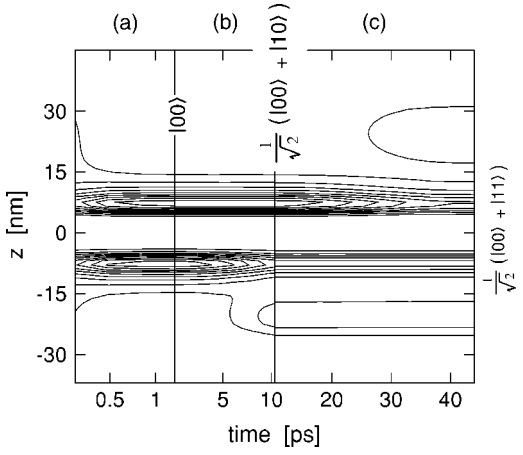

FIG. 10. Contour plots of the electron probability density as functions of time t and spatial coordinate $z=z_1$ for the entanglement process defined by Eq. (8). (a) Relaxation to the ground state, (b) preparation of initial state $(|00\rangle+|10\rangle)\sqrt{2}$, and (c) entanglement production defined by Eq. (8).

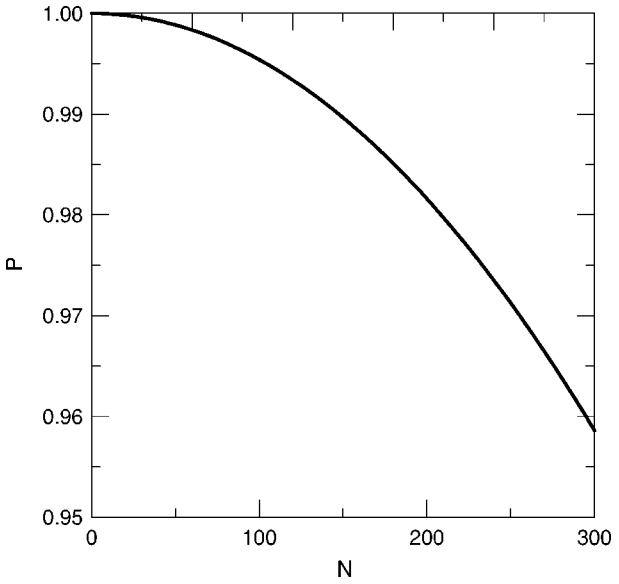

FIG. 11. Probability P of transition from initial state $|10\rangle$ to final state $|11\rangle$ as a function of the number N of gate operations for coherence time $T=1$ ns.

order to perform efficient quantum computations it is necessary to repeat the gate working cycle many times before the decoherence occurs. This poses certain bounds on the CNOT gate operation time. If the quantum transitions were ideally energetically selective, then the application of the π pulse would transform the two-electron system into the appropriate final state with probability 1. However, the ideal quantum transitions could occur only in the limit $t_\pi \to \infty$, i.e., for very small wave amplitude. If the pulse duration time is finite, the quantum transition is no longer ideally selective and the required final state is reached with probability less than 1. The π-pulse duration time is limited by the finite coherence time of the qubit. However, before the qubits become affected by the decoherence, a quantum computer has to perform a large number of operations, e.g., in order to apply the error-correcting codes. The optimal π-pulse duration time has to satisfy the condition $t_\pi < T/N$, where T denotes the coherence time and N is the number of gate operations we want to perform during time T. We note that N is proportional to the wave amplitude A. As a result, for fixed coherence time T the probability of reaching the appropriate final state depends on the number N of the required operations.

Performing simulations of the CNOT gate operation for different wave amplitudes A, we have determined this dependence (Fig. 11). For these simulations we have chosen the transition from state $|10\rangle$ to $|11\rangle$ given by Eq. (7c). The probability $P(t)$ of reaching the final state $|11\rangle$ is calculated as follows: $P(t)=|\langle 11|\psi(t)\rangle|^2$. During the gate operation, the probability $P(t)$ increases and reaches the maximal value if the duration time is equal to t_π. We note that for the real transitions $P(t_\pi)<1$. Figure 11 displays probability $P(t_\pi)$ of reaching the proper final state as a function of the number N of operations performed during coherence time T (we have taken $T=1$ ns). If we require the correct transitions to be realized with probability 99.9%, the model QD system can perform merely ~60 gate operations during the coherence time. However, if we lower this limit to 99.0%, the number of gate operations performed before decoherence takes place is increased to ~150.

V. CONCLUSIONS AND SUMMARY

We have simulated the CNOT gate operation by solving the time-dependent Schrödinger equation for a two-electron system confined in double coupled asymmetric QDs. For this purpose we have selected four computational-basis states. We have shown that the quantum CNOT gate can be realized with these states under the assumption of ideally selective quantum transitions. For real nanostructures the existence of additional bound states of the electrons confined in the QD and decoherence put certain limitations on the gate operations. Due to the finite coherence time the gate operation time has to be bound from above, which causes the quantum transitions to cease to be ideally selective, i.e., not only the computational-basis states can be occupied by the electrons. Therefore, the probability of reaching the appropriate final state, which belongs to the computational basis, is less than 1. The simulations performed show that—under the assumption of 99.9% probability of the required transition—the model QD system can perform ~60 gate operations during the coherence time of 1 ns. If, however, according to Ref. [27], we take a less optimistic estimate of the coherence time, i.e., $T \leqslant 70$ ps, the number of completed operations falls down to 4. In each case the estimated numbers of gate operations performed during the coherence time are by several orders of magnitude too small to complete successful quantum computation with the orbital states of electrons confined in coupled QDs. However, the application of spin states of the confined electrons is more promising due to the much longer spin relaxation time [16]. Moreover, if the QD device could transfer its entangled state onto entangled photons [28,29], the scheme proposed in the present paper could have a practical meaning.

In summary, based on time-evolution simulations, we have shown that physical realization of the quantum CNOT gate is possible with coupled asymmetric QDs before the decoherence destroys the information stored in the qubits. We have optimized the parameters of the nanodevice and obtained quantitative estimates of the gate operation time and the probability of reaching the required final state. It appears that—in the considered coupled QD system—the gate operation time is not small enough as compared with the coherence time. Nevertheless, having at disposal a nanodevice that can perform several CNOT operations during the coherence time, we can study its possible application to the recently proposed production of entangled photon states.

ACKNOWLEDGMENT

This paper has been partly supported by the Polish Ministry of Scientific Research and Information Technology in the framework of the solicited Grant No. PBZ-MIN-008/P03/2003.

[1] L. Jacak, P. Hawrylak, and A. Wójs, *Quantum Dots* (Springer-Verlag, Berlin, 1998).
[2] A. Barenco, D. Deutsch, A. Ekert, and R. Jozsa, Phys. Rev. Lett. **74**, 4083 (1995).
[3] D. Loss and D. P. DiVincenzo, Phys. Rev. A **57**, 120 (1998).
[4] G. Burkard, D. Loss, and D. P. DiVincenzo, Phys. Rev. B **59**, 2070 (1999).
[5] A. A. Balandin and K. L. Wang, in *Proceedings of Quantum Computing and Quantum Communications '98, and Lecture Notes in Computer Science* **1509**, edited by C. P. Williams (Springer-Verlag, Berlin, 1999), p. 460.
[6] P. Recher, E. V. Sukhorukov, and D. Loss, Phys. Rev. Lett. **85**, 1962 (2000).
[7] T. Tanamoto, Phys. Rev. A **61**, 022305 (2000).
[8] F. Troiani, U. Hohenester and E. Molinari, Phys. Rev. B **62**, R2263 (2000).
[9] G. D. Sanders, K. W. Kim, and W. C. Holton, Phys. Rev. B **61**, 7526 (2000).
[10] J. H. Oh, D. Ahn, and S. W. Hwang, Phys. Rev. A **62**, 052306 (2000).
[11] J. H. Reina, L. Quiroga, and N. F. Johnson, Phys. Rev. A **62**, 012305 (2000).
[12] H. Sasakura, S. Muto, and T. Ohshima, Physica E (Amsterdam) **10**, 458 (2001).
[13] J. H. Jefferson, M. Fearn, D. L. J. Tipton, and T. P. Spiller, Phys. Rev. A **66**, 042328 (2002).
[14] P. Zhang, X.-G. Li, and X.-G. Zhao, Phys. Lett. A **294**, 108 (2002).
[15] F. Troiani, E. Molinari, and U. Hohenester, Phys. Rev. Lett. **90**, 206802 (2003).
[16] R. Hanson, B. Witkamp, L. M. K. Vandersypen, L. H. Willems van Beveren, J. M. Elzerman, and L. P. Kouwenhoven, Phys. Rev. Lett. **91**, 196802 (2003).
[17] T. M. Buehler, D. J. Reilly, R. Brenner, A. R. Hamilton, A. S. Dzurak, and R. G. Clark, Appl. Phys. Lett. **82**, 577 (2003).
[18] T. Hayashi, T. Fujisawa, H. D. Cheong, Y. H. Jeong, and Y. Hirayama, Phys. Rev. Lett. **91**, 226804 (2003).
[19] W. H. Zurek, Phys. Today **44**(10), 36 (1991).
[20] A. Barenco, C. H. Bennett, R. Cleve, D. P. DiVincenzo, N. Margolus, P. Shor, T. Sleator, J. A. Smolin, and H. Weinfurter, Phys. Rev. A **52**, 3457 (1995).
[21] B. J. Ohlsson, M. T. Björk, A. I. Persson, C. Thelander, L. R. Wallenberg, M. H. Magusson, K. Deppert, and L. Samuelson, Physica E (Amsterdam) **13**, 1126 (2002).
[22] A. Esser, R. Zimmermann, and E. Runge, Phys. Status Solidi B **227**, 317 (2001).
[23] S. Bednarek, B. Szafran, T. Chwiej, and J. Adamowski, Phys. Rev. B **68**, 045328 (2003).
[24] D. DiVincenzo, Phys. Rev. A **51**, 1015 (1995).
[25] K. T. R. Davies, H. Flocard, S. Krieger, and M. S. Weiss, Nucl. Phys. A **342**, 111 (1980).
[26] A. Askar and A. S. Cakmak, J. Chem. Phys. **68**, 2794 (1978).
[27] S. Sauvage, P. Boucaud, R. P. S. M. Lobo, F. Bras, G. Fishman, R. Prazeres, F. Glotin, J. M. Ortega, and J.-M. Gerard, Phys. Rev. Lett. **88**, 177402 (2002).
[28] V. Cerletti, O. Gywat, and D. Loss, e-print cond-mat/0411235.
[29] C. Emary, B. Trauzettel, and C. W. J. Beenakker, e-print cond-mat/0502550.